Astronomy
&
Astrophysics

Coronal loops heated by turbulence-driven Alfvén waves:
A two fluid model

I. O'Neill and X. Li

Institute of Mathematical and Physical Sciences, University of Wales, Aberystwyth, SY23 3BZ, UK
e-mail: ijo98@aber.ac.uk

Abstract. We present the results of a thorough parameter study of coronal loop models in the aim to explore the mechanism behind coronal heating. The two-fluid coronal loops described in this paper have lengths from 10 Mm to 600 Mm and consist of protons and electrons. The loops are treated with our unique, self-consistent, steady state dynamic loop model to derive the basic parameters (as introduced by Li & Habbal 2003, ApJ, 598, L125). The only heating mechanism assumed is turbulently generated Alfvén waves that carry the necessary flux from the chromosphere to energize the coronal plasma through preferential heating of the proton gas. Strong Coulomb coupling allows energy to pass efficiently from protons to electrons. We have control over the independent variables, driving scale (l) and Alfvén amplitude (ξ), which influence the dissipation and flux of these resonant waves. We find "mapping" the loop parameter response to varying l with fixed ξ a useful tool to find where certain conditions for each loop length exist. From this, we are able to pin-point where the coldest solution lies. For a loop of $L = 10$ Mm, the coolest loops have a maximum temperature of $T = 0.75$ MK. We also focus on a $L = 40$ Mm loop and vary both l and ξ so we can compare results with existing work. From this parameter mapping we can categorise the loop heating profiles. Our model indicates the existence of footpoint, non-uniformly and quasi-uniformly heated profiles. There is also strong evidence to suggest the same mechanism may apply to hot, SXT loops.

Key words. Sun: corona – Sun: transition region

1. Introduction

It is well known that the lower corona is a highly dynamic and diverse region of the solar environment. Observations by the *Transition Region and Coronal Explorer* (*TRACE*), *Solar and Heliospheric Observatory* (*SOHO*) and *Yohkoh* (Soft X-ray Telescope, SXT) have shown there to be a zoo of coronal structures, that vary in scale, lifetime, variability and luminosity. The revolutionary spatial and temporal resolution of *TRACE* has given us a unique insight to the coronal heating phenomena and the nature of these elegant structures. Although advanced observational data is becoming available, the mechanisms behind the observed coronal heating are poorly understood. For instance, recent observations revealed that EUV loops have flat temperature profiles (Lenz et al. 1999). It is known that the majority of these loops cannot be explained by assuming hydrostatic equilibrium, especially long coronal loops (Klimchuk 1987; Ashwanden et al. 2001; Winebarger et al. 2002), when compared with classical models (Rosner et al. 1978). This is because the observed loops can be several orders of magnitude denser (and brighter) than values expected from hydrostatic models (Winebarger et al. 2003). Steady flows have been detected (Winebarger et al. 2002) and have led to speculation that steady flow may be the answer to these observed "overdense" loops. More recently however,

Patsourakos et al. (2004) demonstrated that a steady plasma flow fails to explain the flat temperature profile and high density for a 300 Mm loop. Further work is obviously needed.

A possible way to enhance the density in coronal loops is momentum deposition by plasma waves. Litwin & Rosner (1998) suggested that Alfvén waves can increase the coronal scale heights and therefore coronal loop densities. Recently, Li & Habbal (2003) developed a coronal heating model that simulates the dissipation of Alfvén waves propagating from one footpoint (at $s = 0$) to the other ($s = L$) due to a fully developed turbulent cascade. The model is successful in producing steady flows, flat coronal temperatures and high electron densities. However, the model is only applied to a relatively short loop ($L = 70$ Mm).

The purpose of this paper is to apply the model developed by Li & Habbal (2003) and Li et al. (2004) to various loops. This is a thorough parameter study to explore the coronal response to this mechanism in various conditions. We study Alfvén waves as they carry a large energy flux due to the high Alfvén velocity in the corona. Studies by Hara & Ichimoto (1999) and other authors strongly imply that Alfvén waves may be present in observational data of coronal loops and play a key role in coronal heating. We therefore simulate asymmetric plasma flow (Noci & Zuccarello 1983; Craig & McClymont 1986) with Alfvén wave dissipation acting as the driving force.

The chromosphere acts as a reservoir of plasma as one footpoint "drains" matter into the corona. The photospheric environment is such that it provides a very efficient connection between the sub-photospheric magnetic field and coronal loops (line-tied) as the high mass density and high conductivity provide a very efficient anchor. Oscillations within the solar body are then readily transmitted through the loop structure. We assume the power spectrum of waves transmitted is maintained by a non-linear turbulent cascade where Alfvén waves interact non-linearly to increase the overall wave frequency, maintaining the wave dissipation through the body of the loop. Observations of non-thermal motions in the corona are attributed to such MHD disturbances (Chae et al. 1998).

2. The model and method

We simulate a thin semi-circular cylindrical tube (of length $L = \pi r$) of magnetic flux projecting from the solar "surface" (photospheric footpoints), through the transition region and into the corona. The gravitational acceleration will therefore vary along the axis of the cylinder. The tube is assumed to consist of bundled small-scale "fibrils" (as observed by the high resolution of *TRACE*) which channel the flow of plasma from one footpoint to the other. Using a full-implicit scheme for a one-dimensional model (Hu et al. 1997), the simulation is allowed to attain steady state before results can be taken. The basic one-dimensional, time dependent equations are summarised from Eqs. (1) to (7).

The time dependent continuity equation can be written as

$$\frac{\partial \rho}{\partial t} + \frac{1}{a}\frac{\partial (\rho v a)}{\partial s} = 0 \tag{1}$$

where ρ is the plasma mass density ($\rho \approx n_p m_p$ as $m_p \gg m_e$), v is the plasma velocity, a is the loop cross section (assumed to be constant) and s is the position along the axis of the loop.

The momentum equation can be written as

$$\frac{\partial v}{\partial t} + v\frac{\partial v}{\partial s} = -\frac{1}{\rho}\frac{\partial (p_e + p_p + p_w)}{\partial s} - g_\parallel \tag{2}$$

where p_e, p_p and p_w are the electron, proton and turbulent wave pressure respectively and $g_\parallel$ is the gravitational component acting on the plasma. $g_\parallel$ is expected to have a maximum deceleration (acceleration) effect on upflowing (downflowing) plasma. Naturally, $g_\parallel = 0$ at the loop apex. Our model is unique in that Alfvén waves are used. These waves will introduce momentum deposition to the loop plasma. Momentum deposition may play a very important role in pulling plasma from the chromosphere to the corona (Li & Habbal 2003).

The electron and proton energy equations can be written as

$$\frac{\partial T_e}{\partial t} + v\frac{\partial T_e}{\partial s} + \frac{2T_e}{3a}\frac{\partial(va)}{\partial s} = \frac{2}{3nk_B a}\frac{\partial}{\partial s}\left[a\kappa_e\frac{\partial T_e}{\partial s}\right]$$
$$+2\nu_{pe}\left(T_p - T_e\right) - \frac{2}{3nk_B}L_{rad} \tag{3}$$

$$\frac{\partial T_p}{\partial t} + v\frac{\partial T_p}{\partial s} + \frac{2T_p}{3a}\frac{\partial(va)}{\partial s} = \frac{2}{3nk_B a}\frac{\partial}{\partial s}\left[a\kappa_p\frac{\partial T_p}{\partial s}\right]$$
$$+2\nu_{pe}\left(T_e - T_p\right) + \frac{2}{3nk_B}Q \tag{4}$$

where T_e and T_p are the electron and proton temperatures, n is the plasma density (plasma quasi-neutrality applies, $n_p \approx n_e = n$), k_B is the Boltzmann constant, κ_e and κ_p are the collision-dominated electron and proton heat flux conductivities ($\kappa_e = 7.8 \times 10^{-7}T_e^{5/2}$, $\kappa_p = 3.2 \times 10^{-8}T_p^{5/2}$; Spitzer 1962). L_{rad} is the radiative energy loss from the loop (for an optically thin plasma as derived by Rosner et al. 1978). This parameter is strongly influenced by the density of electrons. Q however is the heating rate of the dissipating wave, energy is absorbed by the proton gas and emitted by the electron gas. Q can be of the form (Hollweg 1986)

$$Q = \frac{\rho\xi^3}{l} \tag{5}$$

where ξ is the Alfvén wave amplitude and l is the driving scale of the Alfvén waves. We will work under the assumption that the non-thermal velocities (i.e. particle motion that is not thermal in origin) observed by Chae et al. (1998) is the fingerprint of ξ. Chae et al. found that spectral lines observed in the transition region and corona (by the Solar Ultraviolet Measurement of Emitted Radiation, SUMER, on board *SOHO*) exhibit excess broadening of spectral lines beyond thermal broadening. The temperatures analysed in this study range from 2×10^4 K to 10^6 K and the corresponding non-thermal velocities (or ξ) range from 5 km s^{-1} to 30 km s^{-1}. We use the ξ vs. temperature curve for quiet-Sun disk observations plot in Fig. 5 from Chae et al. (1998) to read off the desired temperature and corresponding value of ξ. ν_{pe} is the Coulomb collision frequency given by (Braginski 1965)

$$\nu_{pe} = \frac{16\sqrt{\pi}}{3}\frac{ne^4\ln\Lambda}{m_p m_e}\left[\frac{2k_B T_e}{m_e}\right]^{-3/2}. \tag{6}$$

As the Debye length is small in lower coronal regions ($\approx$1cm; Lenz 1999), ν_{pe} becomes an important parameter as a mechanism to transport energy from protons (energized by resonant Alfvén waves) to the lower mass electrons. $\ln\Lambda$ is the Coulomb logarithm ($\ln\Lambda = 23$ in this study as the lower corona is considered to be collision dominated).

Finally, the Alfvén wave energy equation can be written as

$$\frac{\partial p_w}{\partial t} + \frac{1}{a}\frac{\partial}{\partial s}\left[a\left(1.5v + v_A\right)p_w\right] - \frac{v}{2}\frac{\partial p_w}{\partial s} + \frac{Q}{2} = 0 \tag{7}$$

where p_w is the turbulent pressure (given by $p_w = \rho\xi^2/2$) and v_A is the Alfvén speed in the medium (given by $v_A = B/\sqrt{4\pi\rho}$).

All of the above continuity, momentum and energy equations are solved simultaneously to find steady state solutions.

It is important that a total overview is acquired of the response of this range of loop lengths for different Alfvén amplitudes (ξ) and driving scales (l; with reference to Eq. (5)). Rather than taking "shots in the dark" and guessing at the parameters that are outputted, the maximum temperature (T_{max}), minimum density (n_{min}), maximum velocity (v_{max}) and minimum pressure (p_{min}) are plotted for many steady solutions to the ξ and l independent variables.

This portion of our work will take on 3 sections. As an extension to Li & Habbal (2003), we analyse the response

of a number of different coronal loop lengths (from a "short" 10 Mm to a "long" 600 Mm) to the variables ξ and l. The first section demonstrates the sensitivity of loop length to a range of driving scales ($l = 10-8000$ km) whilst being held at a constant Alfvén wave amplitude ($\xi = 10$ km s^{-1}; corresponding to a footpoint temperature of 20 000 K; Chae et al. 1998). The second section again plots L against l, but the Alfvén amplitude is increased to $\xi = 14$ km s^{-1} (corresponding to a footpoint temperature of approximately 30 000 K). The results of $\xi = 10$ km s^{-1} can be compared with $\xi = 14$ km s^{-1}. In the third section, we focus on one loop length ($L = 40$ Mm) to find the parameter response to both ξ and l variables. It is hoped by "mapping" T_{max}, n_{min}, v_{max} and p_{min}, comparisons can be made with the results of other authors (i.e. Winebarger et al. 2003, ran tests on a $L = 40$ Mm loop and compared their dynamic model results with observation).

As the flux and speed of wave dissipation is changed from one solution to the next, the heating profile is unique for each steady solution computed. The following heating profiles are evident in the data described above:

a) *Quasi-uniform heating*. Wave energy is slowly dissipated, allowing some heating but maintaining a very low plasma flow speed. This solution produces a quasi-uniform heated loop and a symmetrical temperature profile. Uniform heating can only be achieved with our model if the plasma velocity is non-zero, but still very small.

b) *Non-uniform heating*. Wave energy dissipates quicker, leading to moderate heating and faster flow speeds. The temperature profile becomes asymmetric and the heating non-uniform. There is a steady loss in wave energy as the waves propagate along the loop. Observed EUV isothermal loops are thought to be heated non-uniformly. As debated by Schmelz (2002) and Aschwanden (2002), these observations can produce some confusing results. Schmelz report uniform temperature profiles of coronal loops may be a by-product of the simple filter-ratio method used for EIT and *TRACE* loops. Aschwanden disputes this argument explaining that the multi-temperature coronal section of an observed loop arises from contributions from neighbouring (in the line-of-sight) loops of multiple temperatures. For now, isothermal loops are believed to exist. If this is the case, modelling non-uniform heating along the loop appears to improve the comparison with *TRACE* and SUMER data for isothermal loops (Winebarger et al. 2002).

c) *Footpoint heating*. If the conditions are extreme enough, wave energy is rapidly dissipated soon after the waves are launched, thereby producing enhanced heating above the upflowing (left) footpoint. The temperature profile is extremely asymmetric with a maximum temperature at the footpoint.

d) *Temperature inversion*. In this case of extreme footpoint heating, a local "temperature inversion" can occur in the body of the coronal loop (Patsourakos et al. 2004; Mok et al. 1990; Antiochos & Klimchuk 1991). This occurs when most of the wave energy is dumped very quickly in the upflowing footpoint. Plasma will then cool toward the loop apex, producing a local minima in the temperature
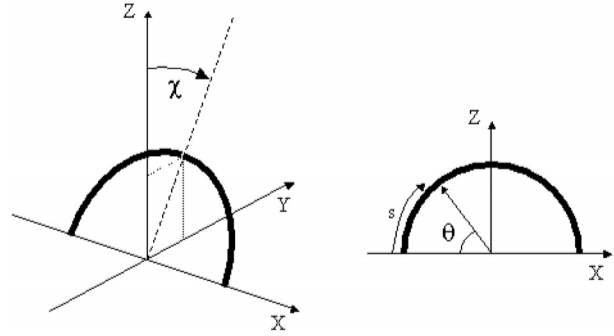

Fig. 1. The geometry used for the inclination, χ, and the arc angle, θ. Refer to Eq. (8) for how these parameters can be applied to coronal loop code.

profile. This effect has been modelled in work by Patsourakos et al. (2004).

The loop structures are not necessarily vertical to the solar surface. Although this can often be assumed to be the case (as the gravity between a vertical and inclined loop may not differ to a great degree, especially for small loops at low altitudes), for extreme inclinations the gravity term may have a greater role to play in loop dynamics. Studies into loop inclination are very important especially when comparing modelled data with observational data (Reale 1999). Aschwanden et al. (2000a) performed a detailed analysis on loops ranging in temperature from 1.5–2.5 MK. It was apparent that for a sample 35 loops, the average inclination was $\approx 30°$ and they ranged from near-vertical to nearly $80°$. From this data, very few loops are close to the assumed perfect vertical projection.

Figure 1 shows the inclination (and arc length, s) in relation to the loop structure. The inclination angle (χ) is taken as the angle from the vertical. As investigated by Tsiklauri & Nakariakov (2001), it was found that the small difference in gravitational acceleration had a large influence on coronal loop dynamics, particularly when considering MHD waves. Of particular interest is how the plasma flow and plasma pressure may be affected by a non-zero χ. The gravity term in Eq. (2) can now be treated as follows:

$$g_{\parallel}(s) = \frac{GM_\odot}{[R_\odot + h(s)\cos\chi]^2} \cos\theta(s)\cos\chi. \qquad (8)$$

It should be noted that there is an extra $\cos\chi$ term in the denominator of Eq. (8). We are dealing with an inclined loop (non-zero χ), therefore there will be a small decrease in the vertical extent (h) of the loop. This will affect the gravity term only very slightly, but has been included for completeness as long loops may be affected strongly by this factor.

In this dynamic model, we assume a steady flow of plasma during the steady state phase of the loop lifetime. We also assume a magnetic field strength of 80G (typical magnetic field strengths in coronal loops are 50−100G; Lenz 1999). The footpoints have a starting temperature of 20 000 K. The wave amplitude, ξ, is fixed at the upflowing footpoint ($s = 0$) but is allowed to change as the waves propagate around the loop. Both footpoints are free boundaries for density and plasma flow velocity, it is the energy flux of the upflowing waves that
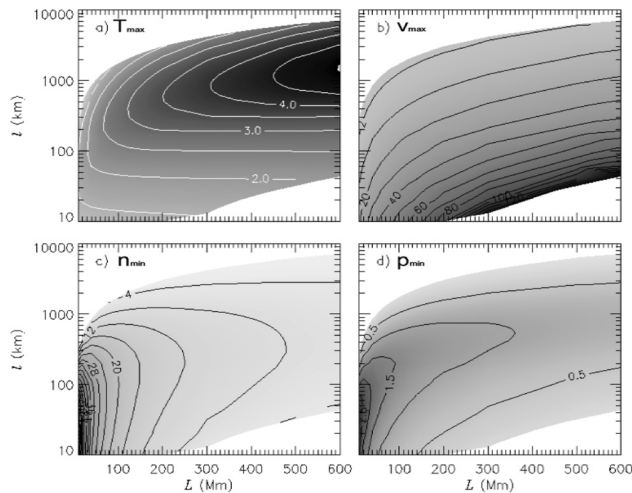
Fig. 2. $\xi = 10 \text{ km s}^{-1}$; **a)** Maximum proton temperature (MK); **b)** maximum proton velocity (km s^{-1}), **c)** minimum proton density ($\times 10^8$ cm^{-3}); **d)** minimum pressure (dyne cm^{-2}).

characterise the coronal loop density and plasma flow. The full-implicit scheme used to evaluate Eqs. (1)–(7) consists of 1160–1350 grid points depending on loop length. The distance between points increases from approx. 15 m at the footpoints to over 1 Mm at the loop apex (for long loops). This provides sufficient resolution for small scale processes low in the corona and expands where large scale processes dominate higher in the corona. For each loop length, a guess is made at the parameters before the numerical method adapts and converges quickly to a steady state. The full-implicit code requires the initial state not to be far from the final solution. If the initial solution should be too extreme (especially when constructing a new initial solution for a unique loop length), an iterative method is applied to slowly adapt the initial solution so the code can compute the desired values of ξ and l. The number of iterations required is dependent on how close the initial guess is to the final solution and how extreme the required values of ξ and l are. The initial guess is therefore independent from the final steady state solution.

3. Results

3.1. Parameter mapping

We can readily simulate warm ($T_{\max} \approx 1$ MK) and dense ($n_{\min} > 10^9$ cm^{-3}) short, EUV loops ($L < 100$ Mm). We also produce hot ($T_{\max} > 2$ MK) and less dense ($n_{\min} \approx 10^9$ cm^{-3}) long, SXT loops ($L > 200$ Mm). Through mapping the coronal loop parameters, we are able to gain an insight to the reaction of loops of a range of lengths to the heating variables.

Figure 2 shows the response of loop lengths $L = 10$–600 Mm to driving scales $l = 10$–8000 km. This range provides us with an overall view on how the plasma parameters react to the l and ξ variables. In this case, all solutions are held at constant $\xi = 10$ km s^{-1}. There are 277 steady solutions that form this analysis. The area with no data in the top left hand corner of each plot are hydrostatic solutions and could not be computed. The area with no data in the bottom right

hand corner are unstable solutions due to extreme plasma flow. Short (long) loops with very high (low) l causes our code to break down. Short loops with very high l lead to insufficient heating near the boundaries to balance the radiative loss. Long loops with very high l may generate supersonic flow and the loop plasma flow will be shocked.

$T_{\max}$, $v_{\max}$, $n_{\min}$ and $p_{\min}$ are plotted in frames a, b, c and d respectively. It is worth noting that these maximum and minimum values are not necessarily at the loop apex. Loops with extreme asymmetry in their heating profiles will cause a heating maximum closer to the loop footpoint. This is not obvious in this figure, but with reference to Fig. 4, generalised regions of heating profiles are plotted. Figure 4 is assembled by scanning through the loop temperature and heating profiles. Temperature inversion, footpoint, non-uniform and quasi-uniform heating profiles are identified according to the profiles evident in Fig. 7. This is produced "by eye" and is only intended to illustrate the general regions of heating profile.

This model predicts generally high plasma temperatures for the whole range of coronal loops, with a maximum value of 5 MK located at $l = 1000$ km for the longest loop, $L = 600$ Mm. The coolest solution is located at $l = 280$ km for a short loop of length $L = 10$ Mm, where the maximum (apex) temperature does not exceed $T = 0.75$ MK. This solution is investigated in Sect. 3.2.

As stated by Li & Habbal (2003) and mentioned by other authors, the driving scale has a strong influence on the mass of plasma flow into the coronal loop (refer to Eq. (5)). Winebarger et al. (2003) use the variable "scale height" (s_H), which is analogous to our driving scale (l). (Winebarger et al. 2003) state a small s_H (and l), has the ability to pull more mass from the chromosphere. This process is reflected in work by Antiochos & Klimchuk (1991), where it is found that an increase in heating (i.e. reducing the driving scale) focuses the energy deposition above the upflowing footpoint, pulling more plasma into the loop. However, Fig. 2c shows that this dependence is not monotonous. For a loop of fixed length, there is a particular value of l which optimises plasma density around the loop apex. For short loops at low l, there is a huge amplification in the apex density, n_{apex} ($n_{\text{apex}} \approx n_{\min}$ in this case). As L is increased, n_{apex} diminishes very quickly. In this case, the density for the shortest ($L = 10$ Mm) loop approaches $n_{\text{apex}} = 8 \times 10^9$ cm^{-3} at low l. However, for the longest loop, $L = 600$ Mm, the density drops to around $n_{\text{apex}} = 4 \times 10^8$ cm^{-3} at low l.

At maximum driving scales, $l_{\max}$, for the whole range of loops, the wave energy seems to be too weak to drive the plasma around the loop, $n_{\min}$ is reduced to a minimum as the plasma flow is close to zero. $l_{\max}$ appears to be highly dependent on L. From this analysis, we can see the contrast between short, cool loops and long, hot loops. We predict cool and very dense loops for $L < 60$ Mm at $l < 100$ km. Also, very hot, less dense loops exist at $L > 200$ Mm, with optimised heating at approximately $l = 1000$ km.

Figure 2 produces densities comparable with *TRACE* and EIT loops (Aschwanden et al. 2000b). We also produce hot X-ray loops with densities comparable with SXT observations (Kano & Tsuneta 1995). Steady flow loop models can
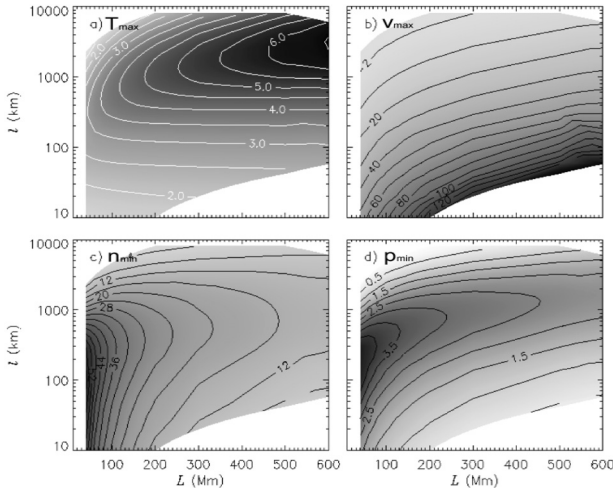
Fig. 3. $\xi = 14$ km s^{-1}. **a)** Maximum proton temperature (MK), **b)** maximum proton velocity (km s^{-1}); **c)** minimum proton density ($\times 10^8$ cm^{-3}); **d)** minimum pressure (dyne cm^{-2}).
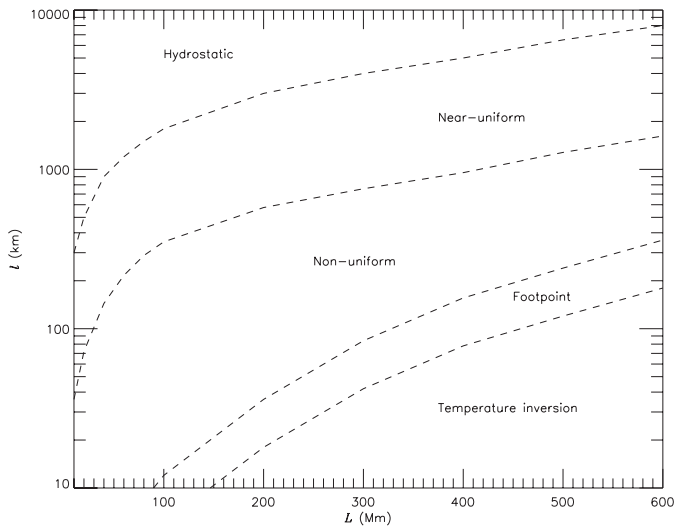

Fig. 4. The regions of loop heating (based on Fig. 2).

enhance loop densities far higher than hydrostatic simulations (Winebarger et al. 2002; Patsourakos et al. 2004) but these models still fail to explain the high density observed by *TRACE*. It is demonstrated here that momentum deposition by Alfvén waves improves the loop densities. This also supports the idea that EUV and SXT loops may share the same (wave-momentum deposition) heating mechanism, as debated by Schmieder et al. (2004). We will return to this important finding in Sect. 3.4.

Figure 3 shows the results for $\xi = 14$ km s^{-1}. A similar pattern as $\xi = 10$ km s^{-1} exists, but more energy is injected into the corona. This effect is demonstrated in the temperature profile (Fig. 3a). The maximum temperature for this range of L has now increased to 6.5 MK, for $L = 600$ Mm at $l = 4000$ km.

This analysis is composed of 285 steady solutions. A greater range of solutions exist; l_{max} has been increased by an average of 62%. The coronal loops are able to support higher driving scales. If ξ is increased, the energy carried by the wave is increased. Therefore, larger driving scales are able to

energize the plasma if the Alfvén amplitude is high enough. This explains why there is such an increase in l_{max} as ξ is raised from $\xi = 10$ km s^{-1} to $\xi = 14$ km s^{-1}.

Although this is the case, for solutions $L < 40$ Mm at $\xi = 14$ km s^{-1}, our code breaks down. As L and l are small, a massive amount of plasma is dragged from the chromosphere to produce very dense coronal loops (Fig. 3c). Although compared to the other solutions in this analysis they appear "cool", these short loops have temperatures in the region of $T < 2$ MK (this is an approximation as loops below $L = 40$ Mm have been ommitted from this plot). If the loop temperature is lowered too far, the solution becomes unstable. Cool loops are a direct result of lower ξ. The maximum density pulled from the chromosphere by Alfvén waves at $\xi = 14$ km s^{-1} is $n_{min} = 6.0 \times 10^9$ cm^{-3}.

Plasma flow velocities along observed steady state coronal loops in active regions are believed to be in the range of $5-16$ km s^{-1} in some solar disk observations (Spadaro et al. 2000) made by SUMER and other *TRACE*/SUMER studies suggest plasma flow speeds of $15-40$ km s^{-1} (Winebarger et al. 2002). Higher velocities have been measured by the Flat Crystal Spectrometer (FCS) on the *Solar Maximum Mission* where plasma velocities were found to be in the range of $40-60$ km s^{-1} (Saba & Strong 1991). In our simulations, if the driving scale is low, higher plasma flow velocities can also be expected. With reference to Fig. 2b and 3b, velocities are enhanced at l_{min} to $v_{max} = 150$ km s^{-1}. Our solutions appear to have a very sharp cut-off at low l where our code breaks down due to the production of shocked plasma flow. The solutions over $L = 200$ Mm demonstrate higher v_{max} for higher l, but the maximum velocity remains below 150 km s^{-1}. Our velocity maximum at low values of l seems very large for quiescent coronal loops. It is suspected that our maximum velocity value may be extreme for these steady, non-flaring loops. Larger l values readily give observed values, small values ($l < 100$ km) do not. With reference to Fig. 4, some footpoint and temperature inversion regions dominate areas of low l values. This suggests that footpoint heating and temperature inversion in highly dynamic loops may be the exception and not the rule. These are interesting features however and shouldn't be discounted from this work.

To further this method, a loop of length $L = 40$ Mm is analysed (Fig. 5). Again, T_{max}, v_{max}, n_{min} and p_{min} are plotted in frames a, b, c and d respectively. We vary ξ and l so we can build a picture as to how a loop of this length responds. 142 steady solutions form this analysis. We choose $\xi = 5-12$ km s^{-1} and $l = 10-1000$ km. The range of ξ corresponds to chromospheric temperatures of $T = 15\,000-22\,000$ K (Chae et al. 1998).

As one would expect, the maximum temperature can be found at maximum ξ (12 km s^{-1}). There is a region of "optimised heating" at approximately $l = 200$ km, lower l tends to cooler solutions. This pattern can be seen for all L, optimised heating occurs at mid-l for each solution, before the code runs into the hydrostatic region (in the top left-hand corner). As observed in Figs. 5a and 5c, a high temperature ($T_{max} = 2.5$ MK) region coincides with a high density ($n = 4.5 \times 10^9$ cm^{-3}) region. This confirms as ξ is increased, greater energy is
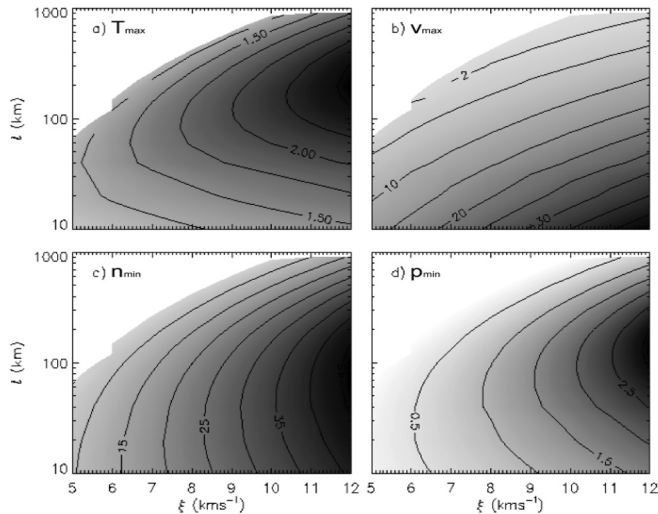
Fig. 5. $L = 40$ Mm. **a)** Maximum proton temperature (MK); **b)** maximum proton velocity (km s^{-1}); **c)** minimum proton density ($\times 10^8$ cm^{-3}); **d)** minimum pressure (dyne cm^{-2}). No data is plotted in the top left hand corner of each plot as these would be hydrostatic solutions and cannot be evaluated by our dynamic code.

Fig. 6. $L = 10$ Mm, "cool" coronal loop heated by Alfvénic turbulence. *Top left*: proton (solid line) and electron (dashed line) temperature along the loop semi-circular length; *top right*: proton velocity (solid), is near-zero and wave amplitude (dashed) appears to remain constant (i.e. little dissipation); *bottom left*: electron density; *bottom right*: wave pressure (top plot) and combined electron and proton pressure (bottom plot). In this simulation, wave amplitude $\xi = 10$ km s^{-1}, and turbulent driving scale $l = 280$ km.

injected into the coronal plasma, causing greater heating and more mass to be driven from the chromosphere. As T and n are in correlation for this test, the total plasma pressure ($p = nkT$) is greatly enhanced at high ξ (Fig. 5d). As can be expected, plasma velocity is high at low l (Fig. 5b), reaching a maximum of $v_{max} = 42$ km s^{-1} at $l = 10$ km and $\xi = 12$ km s^{-1}.

3.2. Short, cool loop solution

To supplement this work, we focus on small-scale structures that have been observed by the high-resolution instrument on *TRACE*. Deep within the chromosphere and low corona, short loops ($L < 10$ Mm) exist at lower temperatures ($T < 1$ MK). Studies by Sakai et al. (2001) investigate these structures and model Alfvén wave production and propagation. It is stated that recent *TRACE* observations have hinted at an unknown energy source within the chromosphere. These small loops readily transmit Alfvén waves excited by footpoint motion to cause heating through reconnection. It seems likely that resonance between MHD waves and plasma may also be a factor in the observed heating, perhaps even amplifying this process in such an extreme environment with high magnetic pressure and high Coulomb coupling. Figure 6 shows a coronal loop of length $L = 10$ Mm in steady state. The driving scale is set to $l = 280$ km and the Alfvén amplitude is $\xi = 10$ km s^{-1} (as the footpoint temperature is 20 000 K, at $s = 0$). From Li & Habbal (2003), it was found that the maximum driving scale allowed was $l = 1350$ km for a loop of length $L = 72$ Mm. However, when modelling a small, $L = 10$ Mm loop, the maximum driving scale allowed by the code is $l = 280$ km. Any attempt at a higher driving scale produces a hydrostatic solution, $v = 0$ km s^{-1}. Once steady state has been achieved at $l = 280$ km, the maximum loop temperature holds at $T = 0.75$ MK, with a perceptible separation of proton and electron temperatures in the coronal section. The minimum (apex) electron
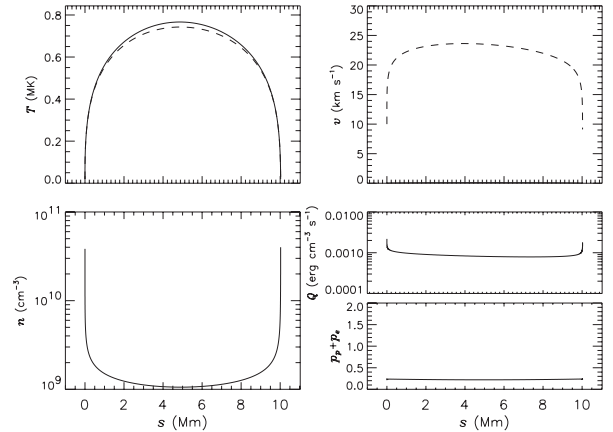
density is $n = 1 \times 10^9$ cm^{-3}. As can be seen in Fig. 6, the solution produces a symmetric velocity and temperature profile about the loop apex. The Alfvén amplitude doesn't change appreciably along the loop length, therefore a uniform heating profile exists during wave propagation. This hinders plasma from being driven from the chromospheric "reservoir" into the loop.

As a comparison, a long loop (of $L = 600$ Mm) is investigated at maximum driving scales. The maximum driving scale for this loop is $l = 7350$ km where the loop tends toward a hydrostatic solution. At this point, the maximum loop temperature is $T = 2.6$ MK and the minimum electron density is $n = 8.4 \times 10^7$ cm^{-3}. As this $l = 7350$ km solution reaches hydrostatic state, the temperature profile again becomes less isothermal, as observed across all loop lengths at l_{max}. As with the short solution at maximum l, there is some separation in electron and proton temperatures. If the driving scale is at the maximum limit, only a small amount of plasma is driven into the loop, reducing loop density, hindering the effect of Coulomb coupling. Therefore, thermal equilibrium between species will be lost in low density regions.

3.3. Loop inclination

Longer coronal loops are more sensitive to variation in inclination angle. Loops of length $L < 200$ Mm show very little difference in parameters when inclined to extreme angles ($\chi > 40°$). However, loops of length $L = 300$ Mm or greater show some decrease in maximum velocity when inclined to angles greater than $\chi = 60°$. This is highlighted when a loop of length $L = 600$ Mm is inclined to 80°. The maximum velocity decreases from 40 km s^{-1} to a little under 30 km s^{-1}. There is a slight increase in heating on the left footpoint and due to the extreme inclination (decreasing the gravity component), the loop pressure tends to an isobaric profile. The maximum

temperature and velocity also deviates from the loop apex toward the left footpoint.

Although this effect is interesting, there is not a large effect on "average" length loops (of length $L \approx 200$ Mm) with modest inclination angles and the effects on more extreme loops are not great. Therefore, assuming a vertical ($\chi = 0$) simulated coronal loop is a good approximation in this study.

3.4. Loop temperature profiles

To supplement our work, we have taken a selection of solutions for a $L = 600$ Mm loop to show the progression of electron temperature and heating rates as l is increased through the different profiles. In this case we use a selection of solutions where $\xi = 14$ km s^{-1}. We have chosen the longest loop and most energetic waves as the features are more obvious when plotted. Figure 7 shows 5 solutions as the driving scale is increased through $l = 60-8000$ km. Each of the heating profile regions are captured in this plot.

Starting at a driving scale of $l = 60$ km, an obvious "dip" is present in the temperature profile. We label this "temperature inversion" in Fig. 4. From the upflowing footpoint to the loop apex, the temperature drops over 1 MK from $T_{max} = 2.5$ MK to $T_{apex} = 1.4$ MK. From the loop apex, there is a slow increase in temperature to $T = 1.75$ MK above the downflowing footpoint. The heating rate is extremely asymmetric indicating a focal point of heating above the upflowing footpoint. Due to high flow velocities it would be easy to mistake the second heating enhancement (above the downflowing footpoint) as kinetic energy transfer to heating. Section 3.5 disputes this in favour of a dominating gravitational energy flux.

As the driving scale is increased to $l = 200$ km, the temperature maximum is again above the upflowing footpoint ($T_{max} = 3.4$ MK), but the "dip" in the temperature profile has decreased significantly. We label this profile "footpoint heating" in Fig. 4. This is a profile where it is obvious there is an enhancement in heating above the upflowing footpoint. The heating rate has also decreased slightly showing that wave energy extends beyond the upflowing footpoint.

At $l = 500$ km, wave energy is able to propagate further without dissipating. In this case, there is a steady loss in wave energy from the upflowing to the downflowing footpoint. The heating rate has decreased further. The maximum temperature has again increased to $T = 4.5$ MK above the upflowing footpoint, but the temperature profile is becoming more symmetric. This profile exhibits a "non-uniform heating" profile. After some experimentation, it was found that by decreasing the energy flux into the loop (ξ), that isothermal solutions are possible. A casestudy is outlined in O'Neill & Li (2004) where the relationship between non-uniform heating and isothermal loops is clarified.

As the driving scale is increased to $l = 2000$ km, optimised heating for the whole loop length is acquired ($T_{max} = 6.3$ MK). The contours in Figs. 2a and 3a show these regions of optimised heating for each loop length. Generally they occur at larger l, before cooler, near-hydrostatic solutions.
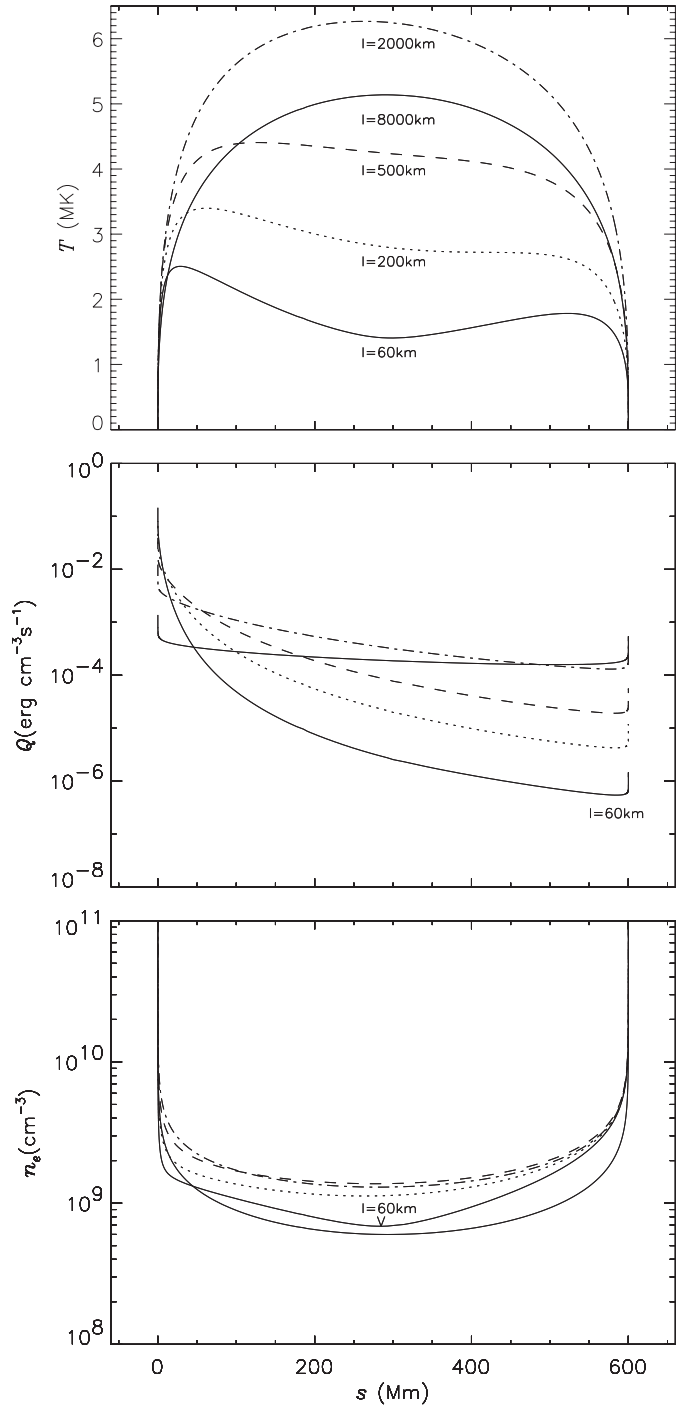

Fig. 7. The temperature (*top*), heating rate (*middle*) and density (*bottom*) progression of a $L = 600$ Mm loop through the driving scales of $l = 60$ (*solid line*), 200 (*dotted*), 500 (*dashed*), 2000 (*dot-dash*) and 8000 km (*triple-dot-dash*). The solid line represents the start of the simulation. Temperature inversion, footpoint, non-uniform, maximum temperature and quasi-uniform heating profiles are all evident.

Higher driving scales ($l = 8000$ km) lead to near-hydrostatic solutions as the maximum temperature settles at $T = 5.2$ MK. The heating rate becomes symmetrical at these large driving scales, therefore driving minimum plasma around the loop, reducing flow and heating.

3.5. Temperature inversion and energy flux

In this section, we check the possible energy fluxes in the loop system using an example of temperature inversion as mentioned in the previous section. In a loop at steady state, the total energy flux is conserved. Equation 9 incorporates the loop's energy flux sources and sinks.

$$\left[\underbrace{\left(3 + \frac{2}{M_A}\right)p_w}_{\text{Wave}} + \underbrace{\frac{\gamma nk\left(T_e + T_p\right)}{\gamma - 1}}_{\text{Enthalpy}} + \underbrace{\int_0^s \frac{nm_p GM_\odot \cos\theta(s)\cos\chi}{\left[R_\odot + h(s)\cos\chi\right]^2}}_{\text{Gravity}}\right.$$

$$\left.+ \underbrace{\frac{1}{2}nm_p v^2}_{\text{KE}}\right]va - \underbrace{\kappa_e a\frac{dT_e}{ds} - \kappa_p a\frac{dT_p}{ds}}_{\text{Conductivities}} + \underbrace{a\int_0^s L_{rad}ds}_{\text{Radiation}} = H \qquad (9)$$

where $M_A = v/v_A$ is the Alfvén Mach number and H is a constant.

As an example, Fig. 8 compares the temperature, velocity and pressure profiles of a 600 Mm loop with the corresponding energy fluxes. This is a vertical loop ($\chi = 0$). The total energy flux (thick solid line in Fig. 8b) remains constant along the whole loop profile suggesting the success (and high accuracy) of our numerical code.

Interestingly, we can readily see how the temperature inversion occurs in loops such as the one shown in Fig. 8. Since the whole loop is powered by Alfvén waves, the wave energy flux dominates the upflowing section as would be expected. The temperature inversion suggests that a strong localized heating process is under way. However, no obvious outstanding external heating is applied (since the wave heating rate is small). During the process of the temperature inversion, the dominant energy flux that can contribute to the heating process is gravity. The radiation loss is small in the coronal part where densities are low. The heat flux and plasma kinetic energy flux are also small when the temperature inversion occurs (Fig. 8b). *It is the release of gravitational energy flux that increases the enthalpy flux.* From this analysis, we can conclude that temperature inversion occurrences are more likely in long vertical loops with low density.

4. Concluding remarks

This paper has provided an overview of the diversity of our dynamic code for a range of loop lengths. By basing our work on the non-thermal motions observed in previous solar studies (Chae et al. 1998), temperatures, densities and velocities are produced that appear to agree with modelled values (Reale et al. 2000; Winebarger et al. 2003; Bradshaw & Mason 2003) and observed values (Aschwanden et al. 2000a; Chae et al. 2000; Spadaro et al. 2000; Winebarger et al. 2002; Saba & Strong 1991). Parameter mapping has proven to be a useful tool when finding a specific solution and limits of our model.

We have explored the limits of the driving scale, l, and found that it is very sensitive to the length of the loop and how
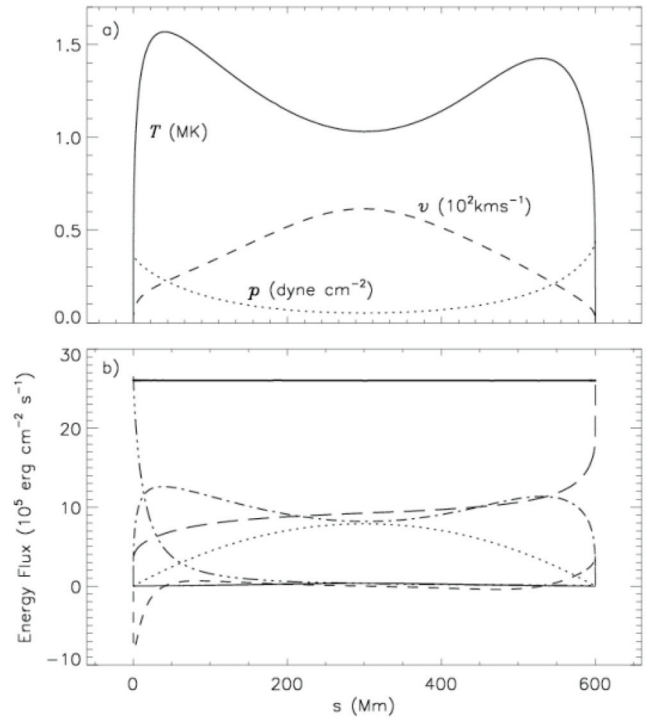

Fig. 8. a) Temperature, velocity and pressure profiles for a 600 Mm (long) loop. $\xi = 6$ km s^{-1} and $l = 40$ km. **b)** Corresponding energy fluxes can be directly compared with the profiles in the top frame. Kinetic energy flux (*thin solid line*), gravitational flux (*dotted*), radiative flux (*long-dash*), conductive flux (*short-dash*), enthalpy flux (*dot-dash*) and wave flux (*triple-dot-dash*) from Eq. (9) will all contribute toward the total flux (*thick solid line*). The total flux must remain constant to confirm steady state.

much energy is provided to the propagating wave by the Alfvén wave amplitude, ξ. The driving scale is poorly understood, but is related to the mean distance between photospheric magnetic flux tubes and granulation (Hollweg 1986).

In this paper, various driving scales (10 km to less than 10 000 km) are used to construct loops with various parameters. At the present time, the detailed process that may excite Alfvén waves in the solar atmosphere is unknown. When the driving scales are in the range of hundreds to thousands kilometres, these scales are in the region of chromospheric granule or supergranule dimensions. When the driving scales are only tens of kilometres, it is not known what features in the solar atmosphere is capable of exciting waves needed and it is beyond the resolution limit of current observations. Li & Habbal (2003) have discussed that the driving scales needed to construct coronal loops need injected waves at frequency of the order of 1 Hz. For very long loops considered in this paper, the frequency may be as large as 0.1 Hz. This perhaps poses a serious challenge to the application of coronal loops heated by turbulent heating. On the other hand, we have to recognize that high frequency waves are difficult to observe with current remote sensing techniques. Sound waves with frequencies of less than 1 minute have been observed (Deubner 1976; Wunnenberg et al. 2002; DeForest et al. 2003). Hence we can speculate that Alfvén waves with similar frequencies may be also abound in the solar atmosphere.

Extreme footpoint heating creates a local minimum at the loop apex for very long loops. If the driving scale is low enough, focused heating at the upflowing footpoint causes a loss in wave energy. This results in cooler plasma flowing through the coronal section of our loops. Plasma velocity is very high as the plasma is accelerated from the upflowing footpoint. Velocity reaches a maximum near the loop apex, where the local temperature minimum is located. As the plasma slows, it would be reasonable to believe kinetic energy is transferred to heating of the plasma. This would have been assumed to be the dominant mechanism heating the right footpoint of long loops with low driving scales. Section 3.5 provides a better understanding of the energy flux responsible for the loop dynamics. Gravity is the most dominant energy source whereas kinetic energy is miniscule.

Experimenting with low values of ξ led to the investigation of isothermal solutions. If the values of ξ and l are balanced correctly, the coronal section of the loop can maintain an isothermal state. Only non-uniform heating can produce this solution. As discussed by Winebarger et al. (2002), non-uniform heating appears to improve the comparison between model result and observations, but further work is required to assess the effects of momentum addition due to waves. This problem is addressed by O'Neill & Li (2004). We find wave heating does indeed improve the loop temperature profile. There is a delicate balance between l and ξ where isothermal solutions are only a small fraction of the total final steady solutions. There is therefore a strong relationship between isothermal loop length and coronal temperature, long loops (>300 Mm) exhibit SXT characteristics whilst short loops (<300 Mm) exhibit EUV temperatures. Further work is required to varify and understand this relationship.

We have built on work by Li & Habbal (2003) to investigate a range of loop lengths. An investigation into loop inclination angle (χ) gave us a useful insight, but the effect of χ on plasma dynamics is small. To improve our model, we will need to investigate varying loop cross section (although a constant cross section is a good assumption for the time being). We only simulated wave propagation from one footpoint to the other. Perhaps symmetric propagation of waves from both footpoints may lead to some interesting results.

There has been no attempt in this paper to directly compare our results with observations of loop profiles. This work is intended to expand on the preliminary studies by Li & Habbal (2003) and Li et al. (2004) but falls short of an exhaustive comparison with recent data. That said, the results of this work are useful when studying the propagation and dissipation of slow MHD waves in coronal loops. Using temperature and density data from observations as a starting point, we can easily produce a steady-state model to further our understanding of slow MHD (or sound) waves in the lower corona. Our ultimate aim is to make direct comparisons of model and observed data so a better understanding of this possible coronal heating mechanism can be attained.

References

Antiochos, S. K., & Klimchuk, J. A. 1991, ApJ, 378, 372

Aschwanden, M. J. 2002, ApJ, 580, L79

Aschwanden, M. J., Alexander, D., Hurlburt, N., et al. 2000a, ApJ, 531, 1129

Aschwanden, M. J., Nightingale, R. W., & Alexander, D. 2000b, ApJ, 541, 1059

Ashwanden, M. J., Schrijver, C. J., & Alexander, D. 2001, ApJ, 550, 1036

Bradshaw, S. J., & Mason, H. E. 2003, A&A, 401, 699

Braginski, S. I. 1965, Rev. Plasma Phys., 1, 205

Chae, J., Schuhle, U., & Lemaire, P. 1998, ApJ, 505, 957

Chae, J., Wang, H., Qiu, J., Goode, P. R., & Wilhelm, K. 2000, ApJ, 533, 535

Craig, I. J. D., & McClymont, A. N. 1986, ApJ, 307, 367

DeForest, C. E., DePontieu, B. D., & Hassler, D. M. 2003, A&AS/Solar Physics Division Meeting, 34,

Deubner, F. L. 1976, A&A, 51, 189

Hara, H., & Ichimoto, K. 1999, ApJ, 513, 969

Hollweg, J. V. 1986, J. Geophys. Res., 91, 4111

Hu, Y. Q., Esser, R., & Habbal, S. R. 1997, J. Geophys. Res., 102, 14661

Kano, R., & Tsuneta, S. 1995, ApJ, 454, 934

Klimchuk, J. A. 1987, ApJ, 323, 368

Lenz, D. D. 1999, ApJ, 517, 497

Lenz, D. D., DeLuca, E. E., Golub, L., Rosner, R., & Bookbinder, J. A. 1999, ApJ, 517, L155

Li, X., & Habbal, S. R. 2003, ApJ, 598, L125

Li, X., O'Neill, I., & Habbal, S. R. 2004, in Waves, Oscillations and Small-Scale Transients Events in the Solar Atmosphere: Joint View from SOHO and TRACE, ESA SP-547: SOHO 13, 279

Litwin, C., & Rosner, R. 1998, ApJ, 506, L143

Mok, Y., Drake, J. F., Schnack, D. D., & van Hoven, G. 1990, ApJ, 359, 228

Noci, G., & Zuccarello, F. 1983, Sol. Phys., 88, 193

O'Neill, I. J., & Li, X. 2004, in SOHO 15 Workshop – Coronal Heating, ESA SP-575

Patsourakos, S., Klimchuk, J. A., & MacNeice, P. J. 2004, ApJ, 603, 322

Reale, F. 1999, Sol. Phys., 190, 139

Reale, F., Peres, G., Serio, S., et al. 2000, ApJ, 535, 423

Rosner, R., Tucker, W. H., & Vaiana, G. S. 1978, ApJ, 220, 643

Saba, J. L. R., & Strong, K. T. 1991, ApJ, 375, 789

Sakai, J. I., Takahata, A., & Sokolov, I. V. 2001, ApJ, 556, 905

Schmelz, J. T. 2002, ApJ, 578, L161

Schmieder, B., Rust, D. M., Georgoulis, M. K., Démoulin, P., & Bernasconi, P. N. 2004, ApJ, 601, 530

Spadaro, D., Lanzafame, A. C., Consoli, L., et al. 2000, A&A, 359, 716

Spitzer, L. 1962, Physics of Fully Ionized Gases (New York: Interscience), 2nd edition

Tsiklauri, D., & Nakariakov, V. M. 2001, A&A, 379, 1106

Winebarger, A. R., Warren, H., van Ballegooijen, A., DeLuca, E. E., & Golub, L. 2002, ApJ, 567, L89

Winebarger, A. R., Warren, H. P., & Mariska, J. T. 2003, ApJ, 587, 439

Wunnenberg, M., Kneer, F., & Hirzberger, J. 2002, A&A, 395, L51